Supplementary Information

Direct cytoskeleton forces cause membrane softening in red blood cells

Ruddi Rodríguez-García[1], Iván López-Montero[1,2], Michael Mell[1,2], Gustavo Egea[3], Nir S. Gov[4] and Francisco Monroy[1,2,*]

[1]Department of Physical Chemistry, Universidad Complutense. Ciudad Universitaria s/n 28040 Madrid, Spain.
[2]Instituto de Investigación Hospital Doce de Octubre (i+12). Avenida de Córdoba, s/n 28041 Madrid, Spain.
[3]Departament of Cell Biology, Immunology and Neurosciences, University of Barcelona, School of Medicine and Instituts d'Investigacions Biomèdiques August Pi i Sunyer (IDIBAPS) and Nanociències i Nanotecnologia (IN^{2}UB), 08036 Barcelona, Spain.
[4]Department of Chemical Physics, Weizmann Institute of Science. Rehovot 76100, Israel.

SI1. Thermal fluctuations of quasi-spherical vesicles

a) Bending modes in the spherical harmonic base: quasi-spherical spectrum. Currently the only membrane geometry whose flickering spectrum can be solved in a purely analytical way is the quasi-spherical vesicle (1). The fluctuating vesicle is assumed with a time-averaged spherical shape with volume and area being conserved quantities. Under this assumption, Milner and Safran considered the fluctuations of a spherical membrane with bending energy given by the Helfrich expression (2):

$$F_{bend} = \frac{1}{2}\kappa \int_S \left(c - c_0\right)^2 dA \qquad \text{(S1.1)}$$

where κ is the bending modulus of the membrane, $c = 1/r_1 + 1/r_2$, the local value of the mean curvature which is defined by two principal radii of curvature and c_0 the spontaneous curvature.

In spherical coordinates, with origin in the centre of the vesicle, assuming the quasi-spherical approach the local radius of the deformed vesicle can be expressed as:

$$r\left(\theta,\varphi,t\right) = R + h\left(\theta,\varphi,t\right) \qquad \text{(S1.2)}$$

where R is the average spherical radius and h the normal displacement.

Since the change in curvature depends only on the normal displacement, h is chosen to express the local curvature and its relative value expanded in spherical harmonics (SH-base):

$$\frac{h(\theta,\varphi,t)}{R}=\sum_{l=m}^{l_{\max}}\sum_{m=2}^{l}U_{lm}(t)Y_{lm}(\theta,\varphi) \qquad \text{(S1.3)}$$

with dimensionless amplitudes $U_{lm}(t)$ given for the SHs defined for the discrete values of the azimuthal (m) and polar (l) integer numbers. The sum starts from $l = m = 2$ because the fundamental swelling mode $l = m = 0$ does not conserve volume and $l = m = 1$ represents a uniform displacement of the center of mass of the entire sphere.

Using this solution, the bending energy in Eq. (S1.1) is minimized with the constraint of constant area, which is treated introducing the membrane tension $\sigma(\Delta)$ as a Lagrange multiplier (2). Within the harmonic approximation for the fluctuation energy, after applying the equipartition theorem for the amplitudes U_{lm}, their quadratic time-averages are obtained as (2):

$$\left\langle U_{lm}^2\right\rangle=\frac{k_BT}{\kappa}\frac{1}{(l+2)(l-1)\left[l(l+1)+\Sigma\right]} \quad \textit{for} \quad l\geq 2, \qquad \text{(S1.4)}$$

with the dimensionless parameter:

$$\Sigma=\frac{\sigma(\Delta)R^2}{\kappa}+4c_0R-2c_0^2R^2 \qquad \text{(S1.5)}$$

accounting for an effective tension that depends of the excess area (Δ) and of the local spontaneous curvature (2). The amplitudes in Eq. (S1.4) represents the quadratic coefficients of the discrete expansion in Eq. (S1.3) using the HS base.

Every spherical harmonics can be viewed as a normal mode of membrane fluctuation in the quasi-spherical object, the 2D-fluctuation geometry of every discrete mode being defined by the degree l and the order m (azimuthal) of the corresponding spherical harmonic. In practice, what is seen under the optical microscope in a flickering experiment is the equatorial cross section of a quasi-spherical membrane. Consequently, only the normal displacements $h(\theta=\pi/2, \varphi, t)$ are measurable along the equatorial contour defined by the variation range of the azimuthal angle $\varphi \in [0, 2\pi]$. As far the quasi-spherical approach is assumed (only one radius defines the average profile), the normal equatorial displacements, in Fourier space, are given by:

$$h(q_m,t)=\frac{1}{2\pi}\int_0^{2\pi}h(\pi/2,\varphi,t)e^{-im\varphi}d\varphi \qquad \text{(S1.6)}$$

with $m = 2, 3, \ldots$) representing the discrete values of the azimuthal number describing the allowed undulations in the circular equator; the discrete wavelengths $\lambda_m = 2\pi R/m$, thus $q_m = 2\pi/\lambda_m = m/R$.

From the expansion in Eq. (S1.3), using the SH base, for a given equatorial mode Eq. (S1.6) re-writes as:

$$h(q_m,t) = \frac{R}{2\pi}\sum_{l=m}^{l_{\max}}\left[U_{lm}(t)\int_0^{2\pi} Y_{lm}(\pi/2,\varphi)e^{-im\varphi}d\varphi\right] \tag{S1.8}$$

where l_{max} is the cut-off number characterizing the fluctuation mode of the shortest possible wavelength. Its order is given by the bilayer thickness, $d \approx 5$nm, thus $l_{max} \approx q_{max} R \approx 2\pi R/d \approx 10^3$.

The amplitude of the equatorial modes can be expressed as a sum of the equatorial projection ($\theta = \pi/2$) of the spherical harmonics over the possible states of polar orientations with wavelengths compatible with the equatorial undulation, *i.e.* with $l \geq m$.

b) Autocorrelation function. In the intent to describe fluctuation dynamics of quasi-spherical membranes to obtain the autocorrelation function (*ACF*), MS considered linear response together with the fluctuation-dissipation theorem and obtained the height-to-height correlations as a progressive sum of exponential decays corresponding to the different spherical harmonics (2). When particularized to the equatorial fluctuations, for the *ACF* one gets:

$$ACF = \langle h(q_m,0)h(q_m,t)\rangle = R^2\sum_{l=m}^{l_{\max}}\langle U_{lm}^2\rangle\, e^{-\omega_l t} \tag{S1.9}$$

where the square amplitude of the *m*-equatorial mode is given by Eq. S1.4 (3,4), and the relaxation frequencies of the discrete modes are given by (1,2):

$$\omega_l(q) = \frac{\kappa}{\eta R^3}\frac{l(l+1)+\Sigma}{Z(l)}, \tag{S1.10a}$$

where *Z(l)* is a geometrical factor given by:

$$Z(l) = \frac{(2l+1)(2l^2+2l-1)}{l(l+1)(l+2)(l-1)} \tag{S1.11}$$

The above formulas describe discrete modes in the quasi-spherical geometry. This imposes periodical boundary conditions which make emerge the quantization rules intrinsic to the spherical harmonics base. However, in the limit of small curvature ($R\rightarrow\infty$), the characteristics of the spherical modes would coincide with solutions in a planar membrane. Indeed, in the limit of high wavevectors (high l, $q \approx l/R$), one has $Z(l) \approx 4/l$ so, in the absence of spontaneous curvature ($c_0 = 0$), the relaxation rates in Eq. (S1.10a) should be found to vary following the approximate formula:

$$\omega_q \approx \frac{\kappa q^3 + \sigma q}{4\eta} \qquad \text{(S1.10b)}$$

which coincides with the well-known expression for the relaxation rate of the bending/tension mode in a planar membrane (5).

This corresponds to a planar mode of wavevector q with elastic energy $F_q \approx \sigma q^2 + \kappa q^4$ (taking Eq. S1.4 in the high-l limit, where $l \approx q/R$), which dissipates energy by viscous friction with the bulk fluid. For a liquid of viscosity η, considering the usual expression of the bulk Oseen tensor; in Fourier space (6):

$$\Lambda_q = \frac{1}{4\eta q} \qquad \text{(S1. 12)}$$

Solving the stochastic equation of motion for the thermal modes of a flexible membrane in a pure viscous fluid (7) (ξ_q is the stochastic field describing a thermal white noise):

$$\frac{\partial h_q}{\partial t} = -E_q \Lambda_q h_q + \Lambda_q \xi_q \qquad \text{(S1.13)}$$

one recovers the relaxation rate in Eq. (S1.10b) as:

$$\omega_q = \Lambda_q E_q = \frac{\sigma q^2 + \kappa q^4}{4\eta q} = \frac{\sigma q + \kappa q^3}{4\eta} \qquad \text{(S1.10b)bis}$$

SI2. Autocorrelation function of the equatorial modes

SI2.a) Fluid membrane vesicles fluctuating in a viscous fluid. In a typical flickering experiment one detects radial deflections in the equatorial plane, which are described as

quadratic amplitudes of the equatorial modes; in terms of the SH base, each equatorial fluctuation characterized by an azimuthal wavevector q_m (= R/m) is described by the discrete sum defined in Eq. (S1.9). The key point is that the dynamic correlations are given by an infinite sum of harmonic contributions projected in the equator, where the summation starts with a fundamental spherical harmonic of equal wavevector than the considered equatorial mode, *i.e.* $l_0 = m$. For pure bending modes ($\sigma \approx 0$; neglecting the spontaneous curvature, $c_0 = 0$ thus $\Sigma \approx 0$), in the continuous approximation*, Eq. (S1.9) can be re-written in the integral form:

$$\left\langle h(q,0)h(q,t)\right\rangle_{bend} \approx R^2 \frac{k_B T}{\kappa} \int_q^\infty \frac{\exp\left[-\left(\kappa q^3/4\eta\right)t\right]}{q^4 R^4} R dq \tag{S2.1}$$

with $dm = R\,dq$.

To perform integration, we consider the change of variable:

$$\begin{aligned} \left(\kappa q^3/4\eta\right)t = \omega_q t = z^3 \\ q\left(\kappa t/4\eta\right)^{1/3} = z \end{aligned} \quad \Rightarrow \quad dq = \left(\kappa t/4\eta\right)^{-1/3} dz \tag{S2.2}$$

Then, Eq. (S2.2) can be rewritten with the simplified form:

$$\left\langle h(q,0)h(q,t)\right\rangle_{bend} \approx \frac{1}{R}\frac{k_B T}{\kappa q^3}\left(\omega_q t\right)\int_z^\infty \frac{e^{-z^3}}{z^4} dz \tag{S2.3}$$

and performing the integration:

$$\int_z^\infty \frac{e^{-z^3}}{z^4} dz = -\left[\frac{e^{-z^3}}{3z^3} - \frac{\mathrm{E}_1\left(z^3\right)}{3}\right]_z^\infty \tag{S2.4a}$$

with the special function $\mathrm{E}_1(x)$ defined as:

$$\mathrm{E}_1(x) = \int_x^\infty \frac{e^{-u}}{u} du\,, \tag{S2.5}$$

* In the continuous approximation to Eq. (S1.9), the integration is performed as the continuous summation under all the possible values of l (= qR), taking now q as a continuous variable instead of the discrete variable l. The integration in Eq. (S2.1) is performed over the "continuous" l, with the differential element being $dl = Rdq$.

which takes the limiting value $E_1(\infty) = 0$; consequently, the integral in Eq. (S2.4a) rewrites as:

$$\int_z^{\infty} \frac{e^{-z^3}}{z^4} dz = \frac{e^{-z^3}}{3z^3} - \frac{\mathrm{E}_1\left(z^3\right)}{3} = \frac{1}{3}\left[\frac{e^{-\omega_q t}}{\omega_q t} - \mathrm{E}_1\left(\omega_q t\right)\right] \tag{S2.4b}$$

Finally, substituting Eq. (S2.4b) in Eq. (S2.3), one finds:

$$\left\langle h(q,0)h(q,t)\right\rangle_{bend} \approx \frac{1}{3R}\frac{k_B T}{\kappa q^3}\left[e^{-\omega_q t} - \left(\omega_q t\right)\mathrm{E}_1\left(\omega_q t\right)\right] \tag{S2.6}$$

The expression in Eq. (S2.6) defines bending-dominated correlations as an exponential decay corrected by the sharply decaying function $E_1(x)$ (see Fig. S1.A). If bending-dominated, the amplitude of the equatorial modes is expected with an effective $\langle h_{eq}^2 \rangle_{bend} \approx (1/3R)\, k_B T/\kappa q^3$ dependence, in agreement with the calculation performed by Pécreaux et al. (4) for the 1D-projection of the rms amplitude of the surface modes projected on the equatorial circumference. Similarly, if membrane tension dominates ($\sigma R^2 >> \kappa$), in the continuous limit Eq. (S2.1) can be expressed as:

$$\left\langle h(q,0)h(q,t)\right\rangle_{tens} \approx \frac{k_B T}{\sigma}\int_q^{\infty} \frac{\exp\left[-\left(\sigma q/4\eta\right)t\right]}{q^2 R^2} R dq\,, \tag{S2.7}$$

which, following the same integration schema as above, can be finally written as:

$$\left\langle h(q,0)h(q,t)\right\rangle_{tens} \approx \frac{1}{R}\frac{k_B T}{\sigma q}\left[e^{-\omega_q t} - \left(\omega_q t\right)\mathrm{E}_1\left(\omega_q t\right)\right] \tag{S2.8}$$

This expression for the correlation function of the tension mode exhibits the same time-dependence as Eq. (S2.6), the corresponding function for bending-dominated modes. However, the equatorial amplitude varies as $\langle h_{eq}^2 \rangle_{tens} \approx (1/R)\, k_B T/\kappa q$, as predicted by Pécreaux et al. (4). To understand the time dependences in Eqs. (S2.6/S2.8) –which are similar in the two different cases (bending/tension modes with bulk friction), the mother expression in Eq. (S2.1) teaches that, when detected at the equatorial plane, the time autocorrelation function (*ACF*) actually corresponds to a summation over all the relaxations existing in the spherical modes that are congruent ($l \geq m$) with the equatorial undulation (characterised by $q_m = m/R$). The sum in Eq. (S2.1) actually superposes a number of exponential decays corresponding to the different *l*-modes projected over the equatorial plane, thus the time dependence of the *ACF* cannot be obtained in a closed

form. From the characteristics of the tension/bending modes in fluctuating membranes with bulk friction, two important properties are deduced for the successive off-plane modes that contribute to a given equatorial undulation: a) they contribute with a decaying amplitude, b) they relax at an increasingly faster rate. Consequently, relaxation of a given equatorial mode (m) should be chiefly dominated by the rate of the master spherical harmonic ($l = m$) with minor contributions from (weaker and faster) higher harmonics ($l > m$). In the case of an incompressible fluid membrane, the relaxation of the equatorial fluctuations in vesicles is described by a time-decay of the functional form:

$$ACF_{tens/bend}^{(eq)} \approx e^{-\omega_q t} - \left(\omega_q t\right) \mathrm{E}_1\left(\omega_q t\right), \qquad \text{(S2.6/S2.8)bis}$$

which is common to modes of the two classes, tension/bending modes with a dissipation due to bulk friction (see Fig. S1A).

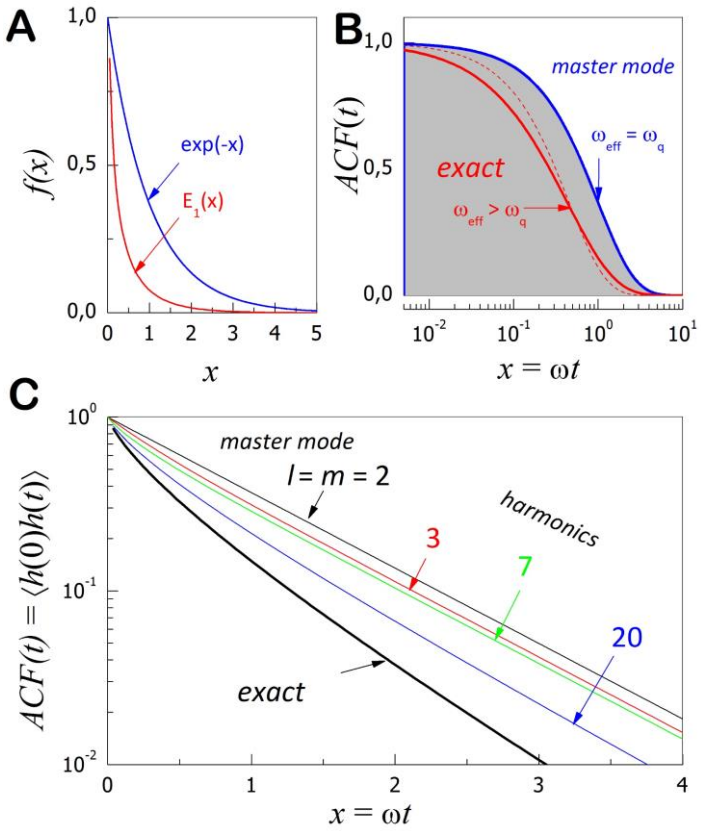

Fig. S1. A) Functional dependence of the relaxation profile of a single spherical mode, (—) f(x) ~ exp(-x), and the summation function accounting from its harmonics, (—) f(x) ~ $E_1(x)$. **B)** ACF-single-exponential master decay of a given equatorial mode (—), compared with its actual relaxation (—), which is a faster with a non-exponential profile affected by all of their higher harmonics present in the grey zone. (- - -) Single exponential of equivalent relaxation time, $\omega_{eff} \approx 1.30\ \omega_q$. **C)** Comparison between the exact solution in Eqs. (S2.6)/(S2.8) for the time dependence of the ACF of equatorial fluctuations in vesicles and the approximate solution to Eq. (S2.1) as truncated series.

The first term of this function corresponds to the master relaxation of the fundamental contribution ($l = m$) to the equatorial mode with $q = m/R$ and relaxation rate ω_q given by Eqs. (S1.12). The second term, which takes-off the exponential decay making it faster, arises from the weighted summation over the higher harmonics ($l > m$). Such contributions give rise to a slight increase of the phenomenological relaxation rates up to an effective value faster than the one expected for the master mode ω_q (see Fig. S1B). This cumulative effect of the higher harmonics was previously discussed by Yoon et al. (8) in the context of RBC flickering, although no analytic solution was explicitly calculated. From the numerical analysis of the cumulative *ACF*, those authors proposed a global relaxation interpolated by a single exponential profile, $ACF(t) \sim \exp[-\omega_q^{(eff)}t]$ with an effective decay rate, $\omega_q^{(eff)} \approx 1.30\ \omega_q$, faster than the master mode (8) (see Fig. SB). However, such a single exponential approximation, albeit successful in describing the relaxation rates, it provides a quite poor description of the exact shape of the cumulative relaxation profile (see Fig. S1B). The multimodal relaxation intrinsic to the observation of the equatorial modes produces a cumulative effect, i.e. the progressively smaller contribution of the faster harmonics at shorter times. In practice, such a heterogeneous relaxation could be accounted for by phenomenological functions, like a "stretched exponential" profile. However, since analytic solutions are available for bending- and tension-governed equatorial fluctuations in vesicles, the experimental *ACF*s should be fitted to the physically significant functions in Eqs. (S2.6) and (S2.8), respectively.

SI2.b) Thermal fluctuations of the RBC membrane. The RBC membrane is significantly more complex than the lipid bilayer in a vesicle. The first theoretical studies emphasized on the global bending stiffness and the bulk viscosity as the two only relevant parameters to explain RBC fluctuations (9,10). The first as the only restoring force exerted by the membrane upon a shape fluctuation. The second as the only viscous parameter relevant to account for frictional dissipation. Obviously, possible intrinsic effects arising from the internal structure of the RBC membrane were almost missed in those models. In the case of RBCs, an underlying cytoskeleton is reinforcing the lipid bilayer, thus shear elasticity must be added as an additional restoring force as well. Furthermore, the coupling between membrane and cytoskeleton must be additionally considered as a confinement contribution which contributes to increase the local value of

the membrane elastic energy upon separating the bilayer from the cytoskeleton. Therefore, the landscape is significantly more complex in RBCs than in bilayer vesicles, so a progressive approximation to the complete physical problem is required, first, considering the indispensable ingredients in a minimal model.

Static spectrum: Planar membrane approximation. In the approximate planar-membrane description, which is exact at high wavevectors, the elastic free energy for a RBC membrane is the sum of the usual Canham-Helfrich Hamiltonian with isotropic bending and tension elastic components describing the elasticity of the fluid membrane plus new terms accounting for the additional contributions of the cytoskeleton, namely, a shear component due to in-plane rigidity and a confinement term, these are:

$$F_{RBC} \approx \frac{1}{2}\left[\sigma\left(\nabla h\right)^2 + \kappa\left(\nabla^2 h\right)^2\right] + \mu\left[2\left(\frac{\partial^2 h}{\partial x \partial y}\right)^2 + \frac{1}{2}\left(\frac{\partial^2 h}{\partial x^2} - \frac{\partial^2 h}{\partial y^2}\right)^2\right] + \frac{1}{2}\gamma h^2 \quad \text{(S2.9)}$$

where the planar strain field (h) is defined as the changes in membrane height with respect to the unstressed reference state in which the membrane is assumed in the flat configuration.

The presence of a rigid cytoskeleton introduces two additional internal components to the elastic response in Eq. (S2.9): **1) in-plane shear**, characterized by a shear modulus (μ) (11) and **2) cytoskeleton confinement**, which makes the free energy to increase with increasing the separation between the membrane and the cytoskeleton (described as a harmonic potential characterized by a spring constant (γ) (12). Since all these new harmonic contributions to the elastic Hamiltonian are summative, in Fourier-space, they contribute altogether as cumulative summands to the effective restoring force. Therefore, similarly to the case of thermal fluctuations in a fluid membrane, considering equipartition of the thermal energy in the different thermal modes, in the planar membrane approximation the spectral amplitudes write as (11,12):

$$\left\langle h_q^2 \right\rangle \approx \frac{k_B T}{\sigma q^2 + \kappa_{eff}\left(q\right) q^4} \quad \text{(S2.10)}$$

with a q-dependent effective bending constant (11):

$$\kappa_{eff}\left(q\right) = \kappa + \frac{9 k_B T}{16\pi\kappa}\mu q^{-2} + \gamma q^{-4} \quad \text{(S2.11)}$$

where the shear contribution is considered in the regime of intermediate q's, where shear modes are effectively decoupled of bending modes (13). In that regime, differently to bending modes whose energy varies as $F_{bend} \sim \kappa q^4$, the energy of the shear contribution goes as $F_{shear} \sim \mu q^2$, similarly to the q-dependence assumed by Sackmann and cols (16) and Brochard and Lennon (14) for the contribution of shear rigidity to the RBC flicker.

Static spectrum: Equatorial fluctuations in the quasi-spherical approximation. Following the seminal work by Brochard and Lennon (14), we will take the sphere as the reference state to describe the equatorial fluctuations of the RBC flicker. Although this is of course only an approximation, it is however adequate to resolve the variational problem of the free energy minimization with a reasonable spherical harmonic base and well adapted to the circular symmetry of the equatorial fluctuations. Therefore, when applied to describe the RBC discocyte, the calculated elastic moduli must be considered as apparent values (not absolute) referred to the hypothetical spherical reference. This consideration was early pointed out by Brochard and Lennon (14), who considered this a reasonable approximation to the RBC flicker. Following the MS description for the bending fluctuations of spherical vesicles and droplets, Faucon et al. (3) discussed the

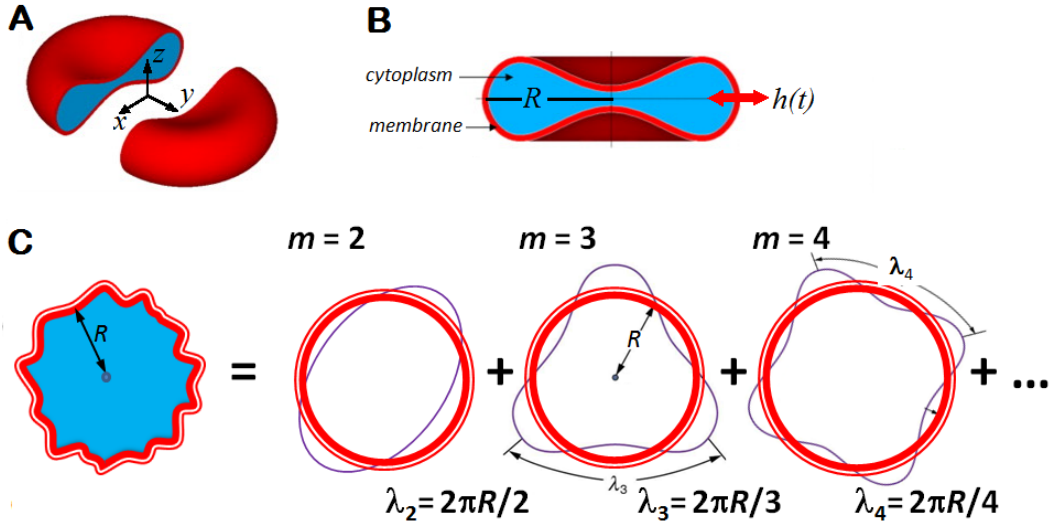

Fig. S2. A) Coordinate system for the quasi-spherical description of the discocyte geometry. **B)** Equatorial geometry: The equatorial modes of fluctuation are described as one-dimensional displacements h(t) with respect to the average radius measured at the equatorial emplacement. **C)** Discrete mode decomposition of the equatorial fluctuations. The equatorial modes are described as the discrete eigen-modes in the circular orbit with wavelengths $\lambda_m = 2\pi R/m$ obtained as integer submultiple of the elemental length $2\pi R$. In the spherical harmonics decomposition, these equatorial eigen-modes correspond to the different values of the azimuthal number m.

limitations of the quasi-spherical method to describe the equatorial flickering of non-

spherical vesicles (see Fig. S2). In practice, one could use the MS expressions with apparent values of the two main mechanical parameters (κ and σ), which must be affected by the other intrinsic characteristics of the membrane due to the presence of the cytoskeleton. Faucon et al. (3) demonstrated that an approximate description of the flickering fluctuations as Fourier modes describes quite accurately the exact MS equations for the quasi-spherical case. So, the quasi-spherical modes with azimuthal wavelength $\lambda_m = 2\pi R/m$ at the equatorial emplacement of average radius R, practically coincide with a Fourier modes of wavenumber $q_m = 2\pi/\lambda_m = m/R$. For $m \geq 5$, they differ very little (by less than the experimental error), which justifies using the much simpler solutions in Eq. (S2.10-S2.11) with the exact MS equations (2). In the quasi-spherical approach to the RBC flicker the equatorial fluctuations are described as a discrete set of spherical harmonics with polar axis parallel to the symmetry normal axis of the discoid cell (15,16). At this quasi-spherical emplacement, the spectrum of the discrete normal modes is given by (2,17):

$$P_m\left(q = m/R\right) = \frac{k_B T}{\kappa_{eff}\left(q\right)} \sum_{l=m} \left\{ \left(l+1\right)\left(l-1\right)\left[l\left(l+1\right) + \Sigma_{eff} \right] \right\}^{-1} \qquad \text{(S2.12)}$$

with effective parameters $\kappa_{eff}(q)$ given by Eq. (S2.11) and Σ_{eff} by Eq. (S1.5). Here, the membrane tension can be effectively reduced by the amount of excess area (Δ). Deviations from the equilibrium curvature should also contribute to create effective surface area eventually increasing fluctuations; in the MS theory this effect is accounted for the curvature parameter c_0 ($c_0 = -2.4$ for the RBC-discocyte shape) (9).

Autocorrelation function. Fluid lipid bilayers in model membranes are usually considered to dynamically behave as an incompressible fluid without internal dissipation. However, the lipid bilayer of real cell membranes is composed by a crowded mixture of lipids and proteins, a molecularly heterogeneous system which is expected with a

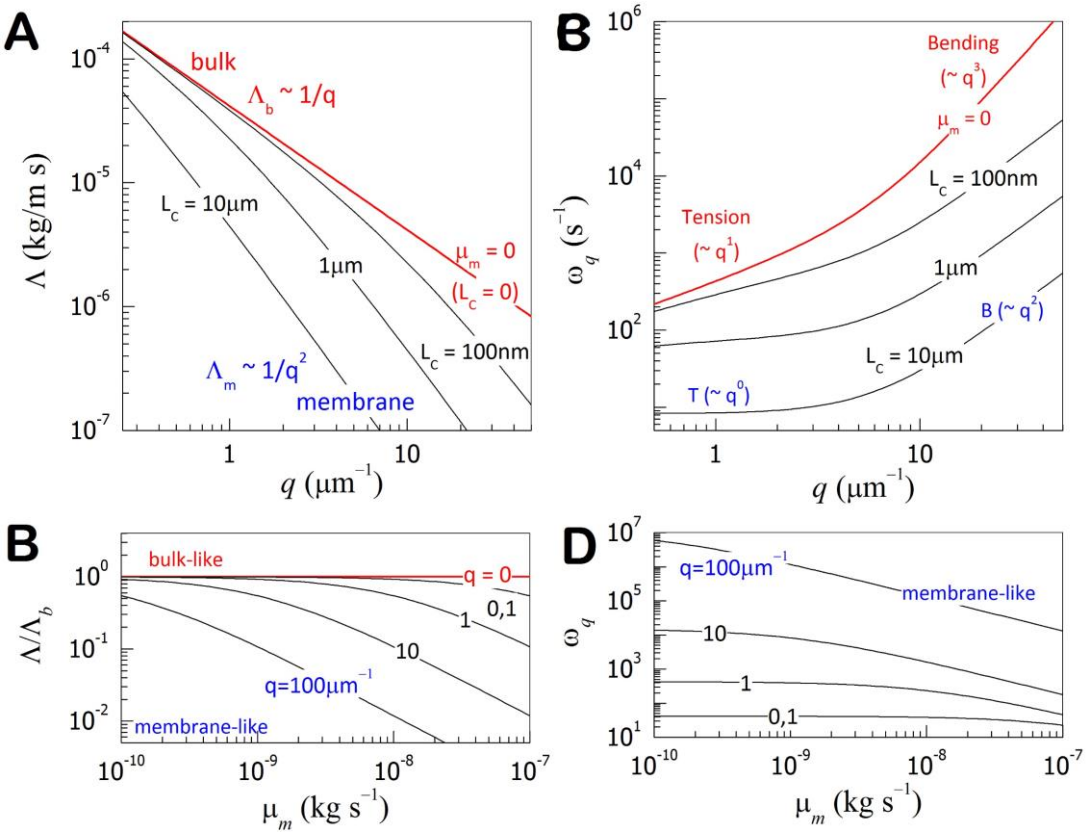

Fig. S3. A) Hydrodynamic compliance as a function of the wavevector. For ideal fluid membrane (zero membrane viscosity, $\mu_m = 0$), one expects a monotonic q-dependence $\Lambda_{bulk} = 1/4\eta q$. As the membrane viscosity increases, also the characteristic length does, $L_C = \mu_m/2\eta$, so one finds renormalization to membrane dominated frictional regime at progressively lower wavevectors, $\Lambda_{memb} \approx 1/2\mu_m q^2$. **B)** Decrease of the hydrodynamic compliance with membrane viscosity. The relative value of the Oseen tensor (with respect to the bulk value) decreases with μ_m, the decrease being progressively faster at higher q. **C)** Dispersion of the tension/bending mode in a membrane with variable membrane viscosity. The typical crossover between tension-like ($\omega_q \sim q$) and bending-dominated ($\omega_q \sim q^3$) modes in a fluid membrane is only observed with zero membrane viscosity ($\mu_m = 0$). The increase of membrane viscosity causes: 1) an absolute decrease of the relaxation rates, 2) a displacement of the tension/bending crossover at smaller wavevectors, and 3) an overall change of the dispersion behavior characterized by a decrease of the dispersion exponents; in the limit of high membrane viscosity ($\mu_m >> 2\eta/q$ or $qL_c >> 1$), the tension mode renormalize to a non-dispersive behavior, $\omega_q \approx \sigma q^0/2\mu_m$, and the bending mode to the membrane-dominated frictional dependence $\omega_q^{(memb)} \approx \kappa q^2/2\mu_m$, comparatively weaker than the bulk-dominated dispersion $\omega_q^{(bulk)} \approx \kappa q^3/4\eta$. **D)** Dependence with membrane viscosity of the relaxation rates of the tension/bending mode. At low wavevectors ($qL_c << 1$), a crossover between a μ_m-independent bulk-like regime and a membrane-like regime is observed. At wavevectors high enough, a monotonous membrane-dominated regime is expected.

comparatively higher intrinsic viscosity than single lipid bilayers. Consequently, significant contributions to frictional dissipation are expected from the internal viscosity of the RBC membrane. Many theoretical works have addressed the hydrodynamics of viscous membranes in the linear flow regime (18,19). In addition to the usual bulk friction accounting for the viscous dissipation of the moving membrane in a bulk fluid of viscosity η, in the simplest approach the membrane is considered a two-dimensional viscous continuum susceptible of planar viscous flow characterized by an intrinsic surface viscosity μ_m. In analogy with the similar tensor for bulk fluids in Eq. (S1.12), the Oseen tensor of the viscous membrane embedded in a bulk fluid is (6,20):

$$\Lambda_q = \frac{1}{4\eta q + 2\mu_m q^2}, \tag{S2.13a}$$

which can be rewritten as the usual bulk hydrodynamic compliance, with an effective value of the bulk viscosity whose q-dependency is determined by the ratio of the intrinsic membrane friction to the bulk friction, this is:

$$\Lambda_q = \frac{1}{4\eta_{eff}(q) q} \quad with \quad \eta_{eff}(q) = \eta\left(1 + \frac{\mu_m q}{2\eta}\right) \tag{S12.13b}$$

The global effect of membrane viscosity on membrane dynamics is to introduce an effective increase of frictional dissipation at spatial scales smaller than a characteristic length, $L_C \approx \mu_m/2\eta$, below which the intrinsic effects of membrane viscosity become dominant. At large distances ($q << L_C^{-1}$), one expects a regular friction governed by the constant value of the bulk viscosity $\eta_{eff} \approx \eta$. However, at short distances ($q >> L_C^{-1}$), the effective viscosity is expected to increase as $\eta_{eff}(q) \approx \mu_m q$, in a thickening regime governed by the intrinsic membrane viscosity. At $q \approx L_C^{-1}$ the hydrodynamic compliance smoothly crossovers from the regular bulk regime into a new frictional regime dominated by membrane viscosity (see Fig. S3). As far the relaxation rates of the modes are determined by the strength of the hydrodynamic compliance, the above described renormalization implies important consequences on the relaxation dynamics depending on the relevant frictional regime. For the sake of simplicity, we first consider the influence of renormalized friction on the relaxation of the pure bending modes. In this particular case, the relaxation rates are expected to renormalize between two limiting regimes:

$$\omega_q = E_q \Lambda_q = \frac{\kappa}{4\eta_{eff}} q^3 \begin{cases} \omega_q^{(bulk)} \approx \dfrac{\kappa}{4\eta} q^3 \quad at \quad q << L_c^{-1} \\ \omega_q^{(memb)} \approx \dfrac{\kappa}{2\mu_m} q^2 \approx \dfrac{\kappa}{4\eta L_C} q^2 \quad at \quad q >> L_c^{-1} \end{cases} \tag{S2.14}$$

In practice, one expects a dispersive behavior in the relaxation rates, $\omega_q \sim q^{2+\alpha}$ with a dispersion exponent $(2+\alpha)$ that renormalizes as $\alpha = 1$ (bulk regular) $\rightarrow 0$ (membrane). If one looks at the equatorial fluctuations, depending on the value of α, the dynamic correlations of the combined spherical harmonics are expected to vary as:

$$\left\langle h(q,0)h(q,t)\right\rangle_{bend} \approx R^2 \frac{k_B T}{\kappa} \int_q^\infty \frac{\exp\left[-\left(\kappa q^{2+\alpha}/4\eta_{eff}\right)t\right]}{q^4 R^4} R dq \tag{S2.15a}$$

Similarly to the integration performed with Eq. (S2.1), we consider the change of variable:

$$\begin{gathered} \left(\kappa q^{2+\alpha}/4\eta_{eff}\right)t = \omega_q t = z^{2+\alpha} \\ q\left(\kappa t/4\eta_{eff}\right)^{1/(2+\alpha)} = z \end{gathered} \quad \Rightarrow \quad dq = \left(\kappa t/4\eta_{eff}\right)^{-1/(2+\alpha)} dz \tag{S2.16}$$

Then, Eq. (S2.15a) can be rewritten with the simplified form:

$$ACF_{bend}(q,\alpha;t) \approx \frac{1}{R}\frac{k_B T}{\kappa q^3}\left(\omega_q t\right)^{3/(2+\alpha)} \int_z^\infty \frac{\exp\left(-z^{2+\alpha}\right)}{z^4} dz\,, \tag{S2.15b}$$

which equals to Eq. (S2.4) in the case of regular friction ($\alpha = 1$).

The integral kernel in the right side of Eq. (2.15b) can be expressed in terms of the special function Generalized Exponential Integral $E_a(x)$ as:

$$\int_z^\infty \frac{\exp\left(-z^{2+\alpha}\right)}{z^4} dz = -\frac{1}{2+\alpha}\left[\frac{E_{(5+\alpha)/(2+\alpha)}\left(z^{2+\alpha}\right)}{z^3}\right]_z^\infty \tag{S2.16a}$$

with the special function $E_a(x)$ defined as:

$$E_a(x) = \int_1^\infty \frac{e^{-xu}}{u^a} du\,, \tag{S2.17}$$

which takes the limiting value $E_a(\infty) = 0$ in the upper limit of the definite integrate in Eq. (S2.16a), so, one gets:

$$\int_z^\infty \frac{\exp\left(-z^{2+\alpha}\right)}{z^4}dz = \frac{1}{2+\alpha}\frac{\mathrm{E}_{(5+\alpha)/(2+\alpha)}\left(z^{2+\alpha}\right)}{z^3}, \tag{S2.16b}$$

which, using the recurrence relation:

$$a\mathrm{E}_{a+1}(x) = e^{-x} - x\mathrm{E}_a(x) \tag{S2.18}$$

converts to:

$$\int_z^\infty \frac{\exp\left(-z^{2+\alpha}\right)}{z^4}dz = \frac{\exp\left(-z^{2+\alpha}\right) - \left(z^{2+\alpha}\right)\mathrm{E}_{3/(2+\alpha)}\left(z^{2+\alpha}\right)}{3z^3} \tag{S2.16c}$$

Therefore, the *ACF* in Eq. (S2.15b) can be re-written as:

$$ACF_{bend}\left(q,\alpha;t\right) \approx \frac{1}{3R}\frac{k_BT}{\kappa q^3}\left[e^{-\omega_q t} - \left(\omega_q t\right)\mathrm{E}_{3/(2+\alpha)}\left(\omega_q t\right)\right], \tag{S2.15c}$$

which exactly coincides with Eq. (S2.6) in the regular case of bulk friction ($\alpha = 1$).

At the opposite limit of non-regular membrane friction ($\alpha = 0$), one has:

$$ACF_{bend}\left(q,\alpha=0;t\right) \approx \frac{1}{3R}\frac{k_BT}{\kappa q^3}\left[e^{-\omega_q t} - \left(\omega_q t\right)\mathrm{E}_{3/2}\left(\omega_q t\right)\right], \tag{S2.19}$$

which is equivalent to the limiting solution of Eq. (S2.15a) in the hydrodynamic regime where membrane viscosity dominates over bulk viscosity ($\eta_{eff} \approx \mu_m q/2$), this is:

$$\left\langle h\left(q,0\right)h\left(q,t\right)\right\rangle_{bend} \approx R^2\frac{k_BT}{\kappa}\int_q^\infty \frac{\exp\left[-\left(\kappa q^2/2\mu_m\right)t\right]}{q^4R^4}Rdq \tag{S2.15d}$$

In this case, making the appropriate change of variable,

$$\begin{aligned}\left(\kappa q^2/2\mu_m\right)t = \omega_q t = z^2 \\ q\left(\kappa t/2\mu_m\right)^{1/2} = z\end{aligned} \quad \Rightarrow \quad dq = \left(\kappa t/2\mu_m\right)^{-1/2}dz \tag{S2.20}$$

after integration, the expression for the ACF takes the asymptotic form:

$$\begin{aligned}&ACF_{bend}\left(q,\alpha=0;t\right) \approx \\ &\approx \frac{1}{3R}\frac{k_BT}{\kappa q^3}\left\{e^{-\omega_q t}\left(1-2\omega_q t\right) + 2\sqrt{\pi}\left(\omega_q t\right)^{3/2}\,\mathrm{erfc}\left(\sqrt{\omega_q t}\right)\right\}\end{aligned} \tag{S2.21}$$

with the special function erfc(x) defined as:

$$\mathrm{erfc}(x) = \frac{1}{\sqrt{\pi}} \int_z^{\infty} e^{-u^2} du \qquad \text{(S2.22)}$$

The expression in Eq. (S2.21) is analytically equivalent to the more compact formula in Eq. (S2.15c), which can be alternatively implemented in fitting algorithms when a hydrodynamic regime dominated by membrane viscosity is expected. In practice, a continuous crossover between bulk controlled ($\alpha = 1$) and membrane dominated ($\alpha = 0$) relaxation is expected with increasing q, thus, for bending-like modes, the time dependence of the ACF is expected with the generalized profile given by Eq. (S2.15c) as a function of the dispersion parameter α, varying as $\alpha = 1 \rightarrow 0$ as q increases.

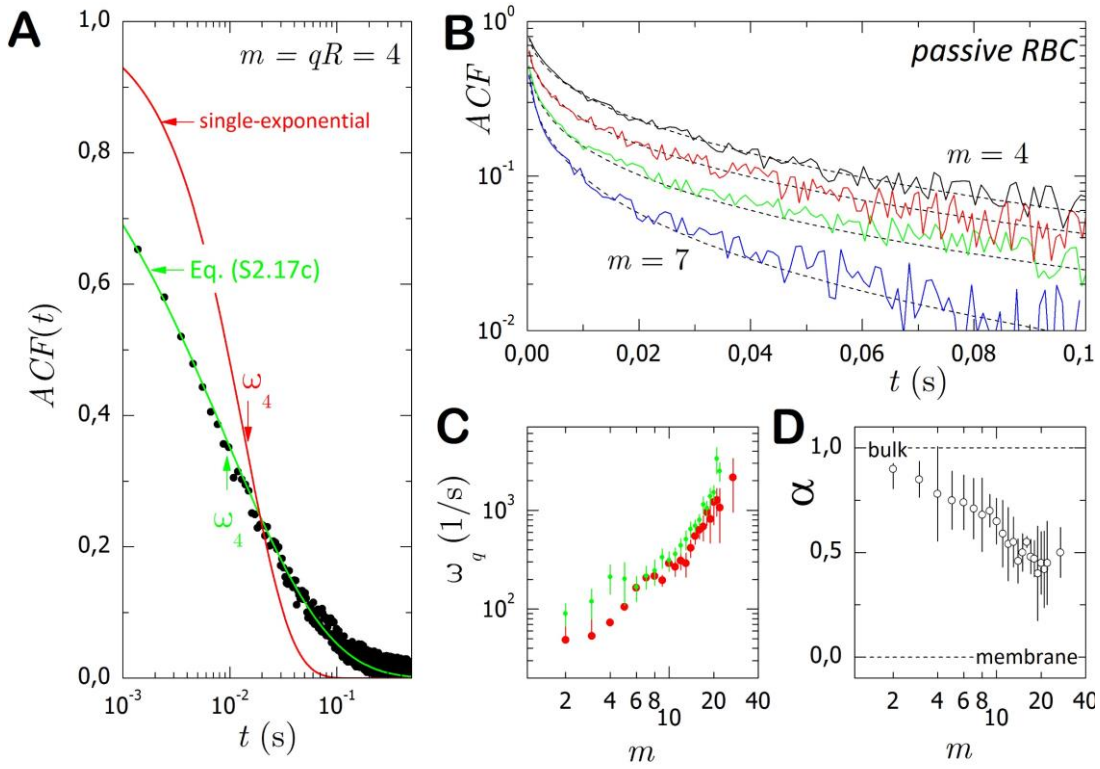

Fig. S4. Experimental autocorrelation function ACF of the passive RBC-flicker. **A)** Typical experimental ACF for m = 4 (symbols) with fits to a single-exponential profile (red) and the exact α–dependent profile in Eq. (S2.17c). The single exponential model is poor in describing the experimental decay and largely overestimates the actual values of the relaxation times (see arrows marking the values of ω_4 obtained from the two models). **B)** Fits of several ACFs of consecutive modes ($m = 4 \rightarrow 7$) to the exact profile in Eq. (S2.17c) (the fitted values of α are plot in D)). **C)** Relaxation rates as obtained from the fits to the single-exponential model (red) and to the exact model in Eq. (S2.17c) (green). Systematically slower rates are obtained with the single-exponential model (red) with respect to the exact decay rates of the experimental profiles (green) obtained from the fits to exact model. **D)** Experimental values of the q-dependent renormalization exponent α describing the effective dispersion of the bending mode $\omega_q \sim q^{2+\alpha}$. As expected a monotonous increase from a bulk-like regime ($\alpha = 1$) down to a membrane-dominated regime is observed with increasing q (α–values from fits in B)).

The results in Figure S4 evidence the adequacy of the α–dependent model to describe the experimental profiles of the ACF of the equatorial thermal modes in the RBC. In particular, Figure S4.A shows a representative ACF for the thermal fluctuations in a drugged RBC ($q = m/R$ with $m = 4$). The experimental relaxation clearly deviates from the single-exponential profile as a stretched-like profile corresponding to a broad distribution of relaxation times rather than to a single relaxation time. The single exponential describe a homogenous relaxation at a rate effectively slower than the phenomenological relaxation rate estimated as an inverse decay time, $\tau^{-1} \approx \omega$ (when $\mathrm{ACF}(t = \tau) = 1/e \approx 0.37$). However, the sum-of-modes function in Eq. (S2.15c) is perfectly able to fit the experimental profiles (see Fig. S4A/B) with relaxation rates higher than those provided by the single-relaxation model (see Fig. S4C) and reasonable values of the dispersion exponent α accounting from effective relaxation between the two limiting frictional regimes, from $\alpha \approx 1$ (bulk friction at low q) down to $\alpha \to 0$ (membrane friction at high q) (see Fig. S4D).

SI3. Power spectral density

The power spectral density (PSD), or simply power spectrum, is a positive real function that measures the frequency content of the stochastic process, this is, how the energy of the signal is distributed with frequency. For a flickering signal $h(t)$, this can be calculated as:

$$PSD(\omega) = \frac{1}{2\pi}\left\| \int_{-\infty}^{\infty} h(t) e^{-i\omega t} dt \right\|^2 \qquad \text{(S3.1)}$$

SI3.a) Experimental determination. In this work, the experimental PSDs were computed from the experimental time series $h(t)$ using Matlab **pwelch** function. The **pwelch** uses the sample rate specified in Hz to compute the PSD and the related frequencies vector in Hz, corresponding to a given temporal trace. The spectral density obtained is calculated in units^2/Hz. Briefly, following the Welch method (21), the algorithm **pwelch** perform the calculation as:

1. The time trace $h(t_i)$ is divided into m overlapping segments (h_k) each with 50% overlap.
2. A Hamming window is applied to each segment h_k
3. An FFT is applied to the windowed data.
4. The (modified) periodogram of each windowed segment is computed $S(e^{i\omega})$
5. The set of modified periodograms is averaged to form the spectrum estimate
6. The resulting spectrum estimate is scaled to compute the power spectral density as $S(e^{i\omega})/fs$ where fs is the sample rate in Hz.

SI3.b) Theoretical model:

Active contribution to the height-height correlation function. We begin with the model of active membranes (12), to calculate the active contribution to the height-height correlation function $ACF_q{}^{(act)}(t)$. This essentially amounts to the inverse Fourier transform of $ACF_q{}^{(act)}(\omega)$ with respect to frequency. In the ideal tensionless state, the function $ACF_q{}^{(act)}(\omega)$ for the direct force mode is (22):

$$ACF_q^{(act)}(\omega) = \langle h(q,\omega)h(-q,\omega)\rangle = n_m p_{on}\left(f_0\Lambda_q\right)^2 \frac{1}{\omega^2+\omega_q^2}\frac{\omega_{act}^{-1}}{1+\left(\omega/\omega_{act}\right)^2} \quad \text{(S3.1)}$$

where n_m is the areal density of motors on the membrane, p_{on} is the probability of a motor to be active at any given time, f_0 is the intrinsic force per motor, Λ_q is the hydrodynamic Oseen tensor for a free membrane, ω_q is the response frequency of the membrane and ω_{act} is the inverse of the mean burst time of each motor. For the curvature-force model f_0 is replaced by $f_0(rq)^2$, where r is the radius of the induced curvature. Fourier transforming we get:

$$\begin{aligned} ACF_q^{(act)}(t) &= \langle h(q,0)h(-q,t)\rangle = \int d\omega \int d\omega' \langle h(q,\omega)h(-q,\omega')\rangle e^{-i\omega t} \\ &= n_m p_{on}\left(f_0\Lambda_q\right)^2 \frac{1}{\left|\omega_{act}{}^2-\omega_q^2\right|}\left(\frac{\omega_{act}}{\omega_q}e^{-\omega_q t}+e^{-\omega_{act}t}\right) \end{aligned} \quad \text{(S3.2)}$$

We see that the active force contributes to the temporal correlations two terms: The first term on the *l.h.s.* of Eq. (S3.2) decays with the membrane natural frequency ω_m, as do the thermal fluctuations (see Eq. (S2.1)). Compared to the thermal fluctuations in Eq. (S1.9), the amplitude of the active correlations with this decay behaviour decreases with increasing wavevector as q^{-11} compared to q^{-4} (for a free membrane and direct force).

This contribution is therefore negligible for all wavevectors where $\omega_q >> \omega_{act}$, which is the case for the current experiments (Fig.1b, right panel). The second contribution in Eq. (S3.2) decays at the natural "frequency" of the motor, ω_{act}. Both contributions diverge when there is a form of resonance, $\omega_q = \omega_{act}$, which does not occur in the red-blood cell case (Fig. 3b; right panel). The divergence in Eq. S3.2 can be eliminated if the time-scale of the active bursts ω_{act} is in fact not completely decoupled from the relaxation modes of the membrane ω_q (which we assumed for simplicity). Such coupling would mean that in fact the resonance-like condition is averted, for example, if long-range (and large-amplitude) slow membrane modes also slow down the rate of active bursts at that wavelength.

Calculation of the height-height PSD. The frequency-dependent power spectral density (PSD) for thermal fluctuations is given by

$$PSD^{(th)} = \left\langle \left| h(\omega) \right|^2 \right\rangle_{th} = \frac{1}{(2\pi)^2} \int \frac{k_B T \Lambda_q}{\omega^2 + \omega_q^2} d^2 q \qquad \text{(S3.3)}$$

The PSD for the direct force model is

$$PSD^{(act)} = \left\langle \left| h(\omega) \right|^2 \right\rangle_{act} = \frac{1}{(2\pi)^2} \int \frac{\left(f_0 \Lambda_q \right)^2}{\omega^2 + \omega_q^2} \frac{p_{on} n_m \omega_{act}^{-1}}{1 + \left(\omega_q / \omega_{act} \right)^2} d^2 q \qquad \text{(S3.4)}$$

We numerically integrate these expressions for the following range of wavevectors: $\pi/L < q < 0.2\text{nm}^{-1}$, where $L = 8\mu\text{m}$ is the lateral size of the RBC membrane. Numerically integrating the PSD for the active component for small−ω, where the tension is dominant, gives the well-behaved function plotted in Fig. 4A.

References

1. Schneider MB, Jenkins JT, Webb WW (1984) Thermal fluctuations of large quasi-spherical bimolecular phospholipid-vesicles. J Phys France, 45:1457-1472.

2. Milner ST, Safran S. (1987) Dynamical fluctuations of droplet microemulsions and vesicles. Phys Rev B 36: 4371-4379

3. Faucon JF, Mitov MD, Méléard P, Bivas I, Bothorel P (1989) Bending elasticity and thermal fluctuations of lipid membranes: Theoretical and experimental requirements. J Phys France 50, 2389-2414

4. Pécreaux J, Dobereiner HG, Prost J, Joanny JF, Bassereau P (2004) Refined contour analysis of giant unilamellar vesicles. Eur Phys J E 13: 277-290

5. Helfrich W (1975) Out-of-plane fluctuations of lipid bilayers. Zeitschrift für Naturforschung. Section C: Biosciences 30: 841.

6. Seifert U and Langer S (1993) Viscous modes of fluid bilayer membranes. EPL (Europhysics Letters) 23: 71.

7. Zilman A and Granek R (1996) Undulations and dynamic structure factor of membranes. Phys Rev Lett 77: 4788-4791.

8. Yoon YZ, Hong H, Brown A, Kim DC, Kang DJ, Lew VL, Cicuta P (2009) Flickering analysis of erythrocyte mechanical properties: dependence of oxigenation, cell shape and hydration level. Biophys J 97: 1606-1615.

9. Deuling H and Helfrich W (1976) Red blood cell shapes as explained on the basis of curvature elasticity. Biophys J 16: 861-868.

10. Waugh R and Evans E (1979) Thermoelasticity of red blood cell membrane. Biophys J 26: 115-131.

11. Lipowsky R, Girardet M (1990) Shape fluctuations of polymerized or solidlike membranes. Phys. Rev. Lett. 65: 2893.

12. Gov N, Zilman AG, Safran S. (2003) Cytoskeleton Confinement and Tension of Red Blood Cell Membranes. Phys Rev Lett 90: 228101-1-4

13. Auth T, Safran SA and Gov NS (2007) Fluctuations of coupled fluid and solid membranes with application to red blood cells. Phys Rev E 76: 051910.

14. Brochard F, Lennon JF (1975) Frequency spectrum of the flicker phenomenon in erythrocytes. J Physique (Paris) 36: 1035-1047.

15. Leibler S, Singh RR, and Fisher ME (1987) Thermodynamic behavior of two-dimensional vesicles. Phys Rev Lett 59:1989-1992.

16. Zeman K, Engelhard H and Sackmann E (1990) Bending undulations and elasticity of the erythrocyte membrane: effects of cell shape and membrane organization. Eur Biophys J 18: 203-219.

17. Huang JS et al. (1987) Study of dynamics of microemulsion droplets by neutron spin-echo spectroscopy. Phys Rev Lett 59: 2600-2603.

18. Hughes BD, Pailthorpe BA, White LR (1981) The translational and rotational drag on a cylinder moving in a membrane. J Fluid Mech 110: 349-372.

19. Lubensky DK and Goldstein RE (1996) Hydrodynamics of monolayer domains at the air–water interface. Phys Fluids 8: 843-854.

20. Camley BA, Brown FLH (2011) Beyond the creeping viscous flow limit for lipid bilayer membranes: Theory of single-particle microrheology, domain flicker spectroscopy, and long-time tails. Phys Rev E 84: 021904

21. Welch P (1967). The use of fast Fourier transform for the estimation of power spectra: a method based on time averaging over short, modified periodograms. Audio and Electroacoustics, IEEE Transactions 15:70-73.

22. Gov NS (2004) Membrane undulations driven by force fluctuations of active proteins. Phys Rev Lett 93: 268104